25th ABCM International Congress of Mechanical Engineering
October 20-25, 2019, Uberlândia, MG, Brazil

COB-2019-0725
ON REAL–TIME FLIGHT SIMULATION OF FLEXIBLE AIRCRAFT WITH INTERPOLATED REDUCED–ORDER MODELS

Juliano Alberto Paulino
Antônio Bernardo Guimarães Neto
Instituto Tecnológico de Aeronáutica
paulino@ita.br
antonio@ita.br

Flávio José Silvestre
Technische Universität Berlin
flavio.silvestre@tu-berlin.de

Andrea Da Ronch
University of Southampton
A.Da-Ronch@soton.ac.uk

Abstract. *Real–time simulation is a valuable tool for aircraft design. However, real–time simulation of flexible aircraft is currently a challenge. This paper presents an approach based on the interpolation of aeroelastic and unsteady aerodynamics reduced–order models in order to reduce simulation time of slightly flexible aircraft models. First, the X-HALE aircraft and model are described, then the interpolated model order reduction technique is presented. Finally, numerical results comparing simulation time histories and duration are presented. Results show a good agreement between full–order and reduced–order model with significant simulation time reduction.*

Keywords: *Flight Simulation, Flexible Aircraft, Aeroelasticity, Reduced–Order Modeling.*

1. INTRODUCTION

The development of modern, more efficient transport aircraft and high altitude long endurance (HALE) aircraft requires lightweight and, consequently, flexible structures. At this point, the rigid–body assumption may not be accurate anymore and coupling between rigid–body and aeroelastic modes must be accounted when modeling flight dynamics.

One problem that arises when modeling flexible aircraft is the high computational cost of such mathematical models. The interaction among unsteady aerodynamics, structural dynamics and flight dynamics results in mathematical models with many state variables and nonlinear equations that can be very computationally expensive (Livne, 2003; Shearer and Cesnik, 2007) and prohibitive to real–time simulation. Even approaches based on linear structural and aerodynamic models can be expensive depending on the effects they represent (Silvestre and Luckner, 2015; Guimarães Neto *et al.*, 2016).

Of particular interest of the current work, real–time simulation of flexible aircraft is highly desirable, but it is currently a challenge. In industry, the benefits provided by real–time flight simulation include the reduction of development costs by using flight simulations instead of flying prototypes, the reduction of development time and the increase of safety by providing pilots ground test and by simulating situations that would be dangerous to be reproduced in a real flight. In academy, flight simulations have been used for control system validation via hardware–in–the–loop simulations (Waszniowski *et al.*, 2011; Kaden *et al.*, 2013), to evaluate aircraft handling qualities (González *et al.*, 2010) and to investigate pilot–induced oscillations (Kish *et al.*, 1996), to cite a few examples.

In face of the challenge of real–time simulation of flexible aircraft and motivated by all the benefits mentioned above, this paper describes an approach for deriving reduced–order approximations of a flexible aircraft flight dynamics model, that are fast enough for real–time simulations while keeps most of aeroelastic key features.

In previous work, we have successfully applied the model order reduction technique to derive local approximations of flexible aircraft flight dynamics models (Paulino *et al.*, 2017, 2018). The objective of the present paper is to use interpolation of reduced–order models in order to expand the good results of local approximations to a wider envelope.

2. X-HALE AIRCRAFT

The X–HALE is a flexible, remotely piloted aircraft developed by Professor Carlos Cesnik and coworkers at the University of Michigan to provide a platform for collecting data that to be used in support for validation of coupled aeroelastic and flight dynamics formulations. It is also intended to be used as a platform for nonlinear control laws tests (Cesnik *et al.*, 2012).

The X–HALE consists in a wing–boom–tail aircraft designed to have a modular airframe that allows it to be mounted in three configurations: slightly flexible (4m wingspan and aspect ratio equal to 20), moderately flexible (6m wingspan and aspect ratio equal to 30) and highly flexible (8m wingspan and aspect ratio equal to 40).

The wing profile is an EMX–07 reflexed airfoil with constant chord length equal to 0.2m along the wingspan with an incidence angle equal to 5 degrees. In all three configurations, the outermost wing panels have 10 degrees dihedral angle and are equipped with trailing–edge control surfaces.

The tails comprise NACA–0012 symmetric airfoils with chord length equal to 0.11m. The central tail can be set to vertical or horizontal configuration only, to increase or decrease lateral–directional stability, respectively. The outer tails are always in the horizontal configuration and their incidence angle can be controlled, acting as elevators.

Recently, the Instituto Tecnológico de Aeronáutica, in Brazil, built two X–HALE aircraft, one in the 4m wingspan slightly flexible configuration, illustrated by Figure 1(a), and another one in the 6m wingspan moderately flexible configuration, illustrated by Figure 1(b). The slightly flexible aircraft is currently in operation, since 2017 and the moderately flexible configuration is expected to enter into operation in the second semester of 2019. The present work considers the 4m slightly flexible configuration only.

(a) Slightly Flexible Configuration (4m wingspan) (b) Moderately Flexible Configuration (6m wingspan)

Figure 1. X-HALE aircraft built by Instituto Tecnológico de Aeronáutica

3. X-HALE MODEL

The X–HALE model adopted in the current work was implemented by following the methodology proposed by Silvestre (2013), which has already been experimentally validated in flight for the utility aircraft Stemme S15 (Silvestre and Luckner, 2015).

The representation of the flight dynamics including aeroelastic effects is based on the linearized mean–axes formulation, proposed by Waszak and Schmidt (1988) and unsteady aerodynamics is modeled using unsteady strip theory based on Jones's exponential approximation of Wagner function (Wagner, 1925).

The set of differential equations that describes the aircraft dynamics are given by:

$$\dot{\boldsymbol{V}}|_B = -\boldsymbol{\omega}|_B \times \boldsymbol{V}|_B + \frac{1}{m}\left(\boldsymbol{T}_{BI}\boldsymbol{W}|_I + \boldsymbol{F_{RB}}|_B + \boldsymbol{F_{AE}}|_B + \boldsymbol{F_P}|_B\right) \tag{1}$$

$$\dot{\boldsymbol{\omega}}|_B = -\boldsymbol{J}^{-1}\left(\boldsymbol{\omega}|_B \times \boldsymbol{J}\boldsymbol{\omega}|_B\right) + \boldsymbol{J}^{-1}\left(\boldsymbol{M_{RB}}|_B + \boldsymbol{M_{AE}}|_B + \boldsymbol{M_P}|_B\right) \tag{2}$$

$$\dot{\boldsymbol{r}} = \boldsymbol{T}_{BI}^T \boldsymbol{V}|_B \tag{3}$$

$$\dot{\boldsymbol{\delta}} = -\boldsymbol{\tau}^{-1}\boldsymbol{\delta} + \boldsymbol{\tau}^{-1}\boldsymbol{u_c} \tag{4}$$

$$\begin{bmatrix}\dot{\boldsymbol{\eta}}(t)\\ \ddot{\boldsymbol{\eta}}(t)\end{bmatrix} = \begin{bmatrix}\boldsymbol{0}_{n_e\times n_e} & \boldsymbol{I}\\ \boldsymbol{\Pi_1}(t) & \boldsymbol{\Pi_2}(t)\end{bmatrix}\begin{bmatrix}\boldsymbol{\eta}(t)\\ \dot{\boldsymbol{\eta}}(t)\end{bmatrix} + \begin{bmatrix}\boldsymbol{0}_{n_e\times n_s}\\ \boldsymbol{\Pi_3}(t)\end{bmatrix}\boldsymbol{\lambda}(t) + \begin{bmatrix}\boldsymbol{0}_{n_e\times n_x}\\ \boldsymbol{\Pi_4}(t)\end{bmatrix}\boldsymbol{x_{RB}}(t) + \begin{bmatrix}\boldsymbol{0}_{n_e\times n_u}\\ \boldsymbol{\Pi_5}(t)\end{bmatrix}\boldsymbol{\delta}(t) \tag{5}$$

$$\dot{\boldsymbol{\lambda}} = \boldsymbol{\Omega}(t)\boldsymbol{\lambda} + \boldsymbol{\Upsilon}\dot{\boldsymbol{w}}_{\boldsymbol{3/4}}(t) \tag{6}$$

where $\boldsymbol{V}|_{\boldsymbol{B}}$ and $\boldsymbol{\omega}|_{\boldsymbol{B}}$ are the linear and angular velocities of the body reference frame with respect to the inertial reference frame; $\boldsymbol{T_{BI}}$ represents the transformation matrix from the inertial reference frame to the reference body frame; m is the total mass of the aircraft; $\boldsymbol{W}|_{\boldsymbol{I}}$ is the aircraft weight expressed in the inertial reference frame; $\boldsymbol{J}$ is the inertia matrix with respect to the aircraft center of gravity.

The terms $\boldsymbol{F_{RB}}|_{\boldsymbol{B}}$, $\boldsymbol{F_{AE}}|_{\boldsymbol{B}}$, $\boldsymbol{F_P}|_{\boldsymbol{B}}$, $\boldsymbol{M_{RB}}|_{\boldsymbol{B}}$, $\boldsymbol{M_{AE}}|_{\boldsymbol{B}}$ and $\boldsymbol{M_P}|_{\boldsymbol{B}}$ in Equations 23 and 24 represents the forces and moments due to rigid–body motion, aeroelastic deformation and propulsive forces, respectively. Differently from the model used in (Paulino *et al.*, 2018), the model used in the current work can represent stall, the inclusion of this effect increases computational cost significantly.

The rigid–body steady aerodynamic coefficients were calculated using Hedman's Vortex Lattice Method (Hedman, 1965) and XFOIL (Drela, 1989). The data is contained in lookup tables parameterized by Reynolds Number and angle of attack.

The three dimensional vector $\boldsymbol{r}$ represents the position of the aircraft body frame with respect to the inertial frame origin. $\boldsymbol{\delta}$ is the state vector of the actuators, modeled as first order linear systems, where $\boldsymbol{\tau}$ is a diagonal matrix that contains the actuators' time constants; $\boldsymbol{u_c}$ is the control input vector.

The vector $\boldsymbol{\eta}$ contains the set of modal coordinates that represents the aircraft structural dynamics; $\boldsymbol{\lambda}$ is the aerodynamic lag vector and $\dot{\boldsymbol{w}}_{\boldsymbol{3/4}}$ represents the first derivative of the downwash at three quarter chord.

More detailed information about the formulation presented here and how the time variant terms $\boldsymbol{\Pi}_i$, $\boldsymbol{\Omega}$ and $\boldsymbol{\Upsilon}$ and are calculated can be found at (Silvestre, 2013).

The model is composed by $n_{RB} = 12$ state variables that describe rigid–body motion: three translations, three rotations, three Euler angles and three spacial coordinates. The actuator dynamics are represented by $n_\delta = 7$ state variables associated to the three engines, two ailerons and two elevators. The aeroelastic dynamics is represented by $n_{AE} = 30$ state variables and unsteady aerodynamics is represented by $n_\lambda = 220$ state variables, two lag states for each strip of the aerodynamic model. The order of the model described in this section, designated in the remaining of this paper as Full–Order Model (FOM) is $n_{FOM} = n_{RB} + n_\delta + n_{AE} + n_\lambda = 269$.

4. MODEL ORDER REDUCTION

The model order reduction technique employed in the current work was proposed by Da Ronch *et al.* (2012). It was conceived for flight control law design of flexible aircraft. In summary, the technique uses information on the eigenspectrum of the Jacobian matrix and projects the system through a Taylor series expansion onto a small basis of eigenvectors representative of the system dynamics, retaining terms up to third order.

Consider a system with dynamics represented by the state equation:

$$\dot{\boldsymbol{x}} = \boldsymbol{F}(\boldsymbol{x}, \boldsymbol{u}), \tag{7}$$

where $\boldsymbol{F}$ is a nonlinear function, $\boldsymbol{u}$ represents a control or perturbation input vector and $\boldsymbol{x}$ is an n–dimensional state vector.

Consider now $\boldsymbol{\Delta x} = \boldsymbol{x} - \boldsymbol{x_0}$ a small perturbation in the state vector with respect to an equilibrium point $\boldsymbol{x_0}$ and $\boldsymbol{\Delta u} = \boldsymbol{u} - \boldsymbol{u_0}$ a small perturbation in the input vector with respect to the equilibrium point $\boldsymbol{u_0}$. The nonlinear state equation represented by Eq. (7) is expanded in a Taylor series around $\boldsymbol{x_0}$ and $\boldsymbol{u_0}$ and the system dynamics is approximated by:

$$\boldsymbol{\Delta}\dot{\boldsymbol{x}} \approx \boldsymbol{A}\boldsymbol{\Delta x} + \frac{\partial \boldsymbol{F}}{\partial \boldsymbol{u}}\boldsymbol{\Delta u} + \frac{1}{2!}\boldsymbol{B}(\boldsymbol{\Delta x}, \boldsymbol{\Delta x}) + \frac{1}{3!}\boldsymbol{C}(\boldsymbol{\Delta x}, \boldsymbol{\Delta x}, \boldsymbol{\Delta x}), \tag{8}$$

where $\boldsymbol{A}$, $\boldsymbol{B}$ and $\boldsymbol{C}$ represents the first, second and third Jacobian operators defined by:

$$A_{ij} = \frac{\partial F_i(\boldsymbol{x_0})}{\partial x_j}, \tag{9}$$

$$B_i(\boldsymbol{a}, \boldsymbol{b}) = \sum_{j,k=1}^{n} \frac{\partial^2 F_i(\boldsymbol{x_0})}{\partial x_j \partial x_k} a_j b_k, \tag{10}$$

$$C_i(\boldsymbol{a}, \boldsymbol{b}, \boldsymbol{c}) = \sum_{j,k,l=1}^{n} \frac{\partial^3 F_i(\boldsymbol{x_0})}{\partial x_j \partial x_k \partial x_l} a_j b_k c_l. \tag{11}$$

The Taylor series expansion (8) is then projected onto a small basis formed by m ($m \ll n$) eigenvectors of the Jacobian matrix $\boldsymbol{A}$ which are representative of the aircraft dynamics. Denote $\boldsymbol{\phi_i}$ and $\boldsymbol{\psi_i}$ the right and left eigenvectors of $\boldsymbol{A}$, i.e.,

$$\boldsymbol{A}\boldsymbol{\phi_i} = \lambda_i \boldsymbol{\phi_i}, \quad \text{for } i = 1, ..., n, \tag{12}$$

$$\boldsymbol{A}^T\boldsymbol{\psi_i} = \bar{\lambda}_i\boldsymbol{\psi_i}, \quad \text{for} \;\; i = 1, ..., n. \tag{13}$$

It is convenient that the set of eigenvectors that forms the reduced–order model basis satisfies the biorthonormality conditions, i.e.,

$$\langle \boldsymbol{\phi_i}, \boldsymbol{\phi_i} \rangle = 1, \quad \text{for} \;\; i = 1, ..., m, \tag{14}$$

$$\langle \boldsymbol{\psi_j}, \boldsymbol{\phi_i} \rangle = \delta_{ij}, \quad \text{for} \;\; i = 1, ..., m, \tag{15}$$

$$\langle \boldsymbol{\psi_j}, \bar{\boldsymbol{\phi}}_i \rangle = 0, \quad \text{for} \;\; i = 1, ..., m, \tag{16}$$

where δ_{ij} represents the Kronecker delta and the inner product is defined as $\langle \boldsymbol{a}, \boldsymbol{b} \rangle = \bar{\boldsymbol{a}}^T\boldsymbol{b}$. Now, consider the transformation of coordinates:

$$\boldsymbol{\Delta x} = \boldsymbol{\Phi z} + \bar{\boldsymbol{\Phi}}\bar{\boldsymbol{z}}, \tag{17}$$

where

$$\boldsymbol{\Phi} = \begin{bmatrix} \boldsymbol{\phi_1} & \boldsymbol{...} & \boldsymbol{\phi_m} \end{bmatrix} \tag{18}$$

and $\boldsymbol{z} \in \mathbb{C}^m$ is the reduced–order model state variable vector. Applying the transformation of coordinates (17) into Eq. (8) and then premultiplying each term by the conjugate transpose of the left modal matrix, results in:

$$\bar{\boldsymbol{\psi}}_j^T(\boldsymbol{\phi_i}\dot{z}_i + \bar{\boldsymbol{\phi}}_i\dot{\bar{z}}_i) = \bar{\boldsymbol{\psi}}_j^T\Big(\boldsymbol{A\phi_i}z_i + \boldsymbol{A}\bar{\boldsymbol{\phi}}_i\bar{z}_i + \frac{\partial \boldsymbol{F}}{\partial \boldsymbol{u}}\boldsymbol{\Delta u} + \frac{1}{2!}B_i(\boldsymbol{z}, \boldsymbol{z}) + \frac{1}{3!}C_i(\boldsymbol{z}, \boldsymbol{z}, \boldsymbol{z})\Big). \tag{19}$$

Once the biorthonormality conditions (14), (15) and (16) were satisfied, the set of m equations (19) can be simplified as

$$\dot{z}_i = \lambda_i z_i + \boldsymbol{\psi}_j^T\Big(\frac{\partial \boldsymbol{F}}{\partial u}\boldsymbol{\Delta u} + \frac{1}{2!}B_i(\boldsymbol{z}, \boldsymbol{z}) + \frac{1}{3!}C_i(\boldsymbol{z}, \boldsymbol{z}, \boldsymbol{z})\Big), \tag{20}$$

where the bilinear and trilinear terms are written as

$$B_i(\boldsymbol{z}, \boldsymbol{z}) = \sum_{r,s=1}^{m} B_i(\boldsymbol{\phi_r}, \boldsymbol{\phi_s})z_r z_s + B_i(\boldsymbol{\phi_r}, \bar{\boldsymbol{\phi}}_{\boldsymbol{s}})z_r\bar{z}_s + B_i(\bar{\boldsymbol{\phi}}_{\boldsymbol{r}}, \boldsymbol{\phi_s})\bar{z}_r z_s + B_i(\bar{\boldsymbol{\phi}}_{\boldsymbol{r}}, \bar{\boldsymbol{\phi}}_{\boldsymbol{s}})\bar{z}_r\bar{z}_s \tag{21}$$

and

$$\begin{aligned} C_i(\boldsymbol{z}, \boldsymbol{z}, \boldsymbol{z}) = \sum_{r,s,t=1}^{m} \Big(& C_i(\boldsymbol{\phi_r}, \boldsymbol{\phi_s}, \boldsymbol{\phi_t})z_r z_s z_t + C_i(\boldsymbol{\phi_r}, \boldsymbol{\phi_s}, \bar{\boldsymbol{\phi}}_{\boldsymbol{t}})z_r z_s\bar{z}_t + C_i(\boldsymbol{\phi_r}, \bar{\boldsymbol{\phi}}_{\boldsymbol{s}}, \boldsymbol{\phi_t})z_r\bar{z}_s z_t + \\ & C_i(\boldsymbol{\phi_r}, \bar{\boldsymbol{\phi}}_{\boldsymbol{s}}, \bar{\boldsymbol{\phi}}_{\boldsymbol{t}})z_r\bar{z}_s\bar{z}_t + C_i(\bar{\boldsymbol{\phi}}_{\boldsymbol{r}}, \boldsymbol{\phi_s}, \boldsymbol{\phi_t})\bar{z}_r z_s z_t + C_i(\bar{\boldsymbol{\phi}}_{\boldsymbol{r}}, \boldsymbol{\phi_s}, \bar{\boldsymbol{\phi}}_{\boldsymbol{t}})\bar{z}_r z_s\bar{z}_t + \\ & C_i(\bar{\boldsymbol{\phi}}_{\boldsymbol{r}}, \bar{\boldsymbol{\phi}}_{\boldsymbol{s}}, \boldsymbol{\phi_t})\bar{z}_r\bar{z}_s z_t + C_i(\bar{\boldsymbol{\phi}}_{\boldsymbol{r}}, \bar{\boldsymbol{\phi}}_{\boldsymbol{s}}, \bar{\boldsymbol{\phi}}_{\boldsymbol{t}})\bar{z}_r\bar{z}_s\bar{z}_t \Big) \end{aligned} \tag{22}$$

It is possible to calculate all the bilinear and trilinear contributions without calculating all the second and third order partial derivatives analytically. They can be approximated by using finite differences instead. The bilinear and trilinear contributions consist, in general, of $4m^2$ and $8m^3$ terms. However, it is possible to reduce the number of terms to $2m^2+m$ and $\frac{2}{3}(2m^3 + 3m^2 + m)$ respectively by exploiting the symmetry of the Jacobian operators (Da Ronch *et al.*, 2012).

5. INTERPOLATED REDUCED–ORDER MODEL

In a previous work (Paulino *et al.*, 2018), we have successfully applied the model order reduction technique described in Section 4 to the Eq. 5 and Eq. 6 of the aircraft model, retaining the linear terms only, in order to approximate the most expensive and highest order set of equations that describe the aircraft behavior, while maintaining the rigid–body equations of motion, which are highly nonlinear, but computationally cheap, untouched. Although this approach showed good results, allowing us to simulate a number of maneuvers, such as surfaces doublets and coordinate curves, that approximation fails when the operation velocity changes significantly. Figure 2 illustrates this behavior, by showing the wing tip displacement due to an smooth increase in the aircraft velocity from 15 m/s to 19 m/s.

This discrepancy happens because a single linear reduced–order model (ROM) was used to represent the aircraft aeroelastic dynamics in the entire envelope. As velocity changes and moves away from operating point where ROM was generated, the approximation becomes worse.

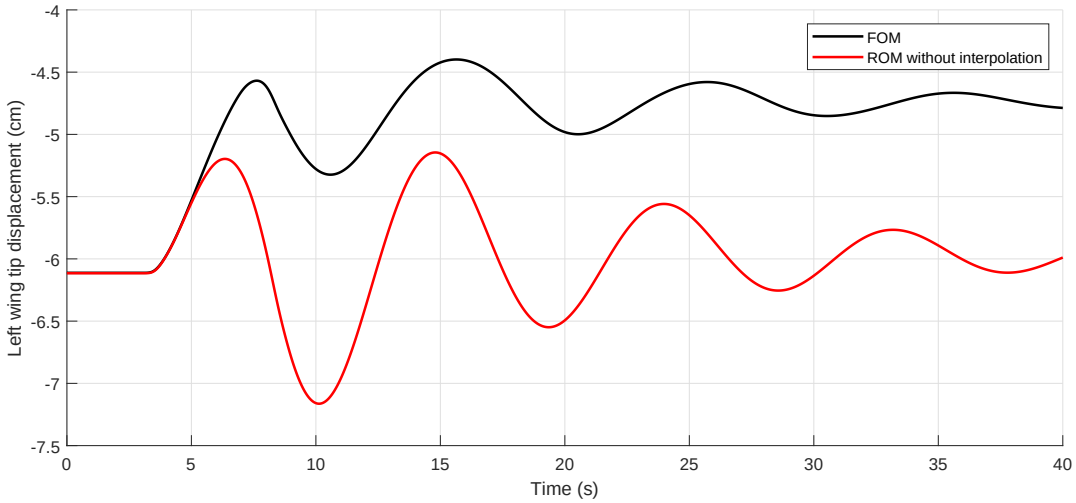

Figure 2. Comparison between FOM and ROM (without interpolation) left wing tip displacement due to a smooth change in velocity from 15 m/s to 19 m/s.

In order to overcome this limitation, a set of ROMs was generated for different operation velocities covering the range between 13 m/s and 19 m/s in steps of 1 m/s for the aeroelastic and aerodynamic lag equations. During simulation time, the respective first derivatives are calculated as a linear combination of the responses of the two closest ROMs.

The state equations of the reduced–order model are expressed as:

$$\dot{\boldsymbol{V}}|_B = -\boldsymbol{\omega}|_B \times \boldsymbol{V}|_B + \frac{1}{m}\left(\boldsymbol{T}_{BI}\boldsymbol{W}|_I + \boldsymbol{F_{RB}}|_B + \tilde{\boldsymbol{F}}_{\boldsymbol{AE}}|_B + \boldsymbol{F_P}|_B\right) \tag{23}$$

$$\dot{\boldsymbol{\omega}}|_B = -\boldsymbol{J}^{-1}\left(\boldsymbol{\omega}|_B \times \boldsymbol{J}\boldsymbol{\omega}|_B\right) + \boldsymbol{J}^{-1}\left(\boldsymbol{M_{RB}}|_B + \tilde{\boldsymbol{M}}_{\boldsymbol{AE}}|_B + \boldsymbol{M_P}|_B\right) \tag{24}$$

$$\dot{\boldsymbol{r}} = \boldsymbol{T}_{BI}^T \boldsymbol{V}|_B \tag{25}$$

$$\dot{\boldsymbol{\delta}} = -\boldsymbol{\tau}^{-1}\boldsymbol{\delta} + \boldsymbol{\tau}^{-1}\boldsymbol{u_c} \tag{26}$$

$$\dot{\boldsymbol{z}}_{\boldsymbol{\eta}}|_{ref} = (1-\kappa)\dot{\boldsymbol{z}}_{\boldsymbol{\eta}}^{-}|_{ref} + \kappa\dot{\boldsymbol{z}}_{\boldsymbol{\eta}}^{+}|_{ref} \tag{27}$$

$$\dot{\boldsymbol{z}}_{\boldsymbol{\lambda}}|_{ref} = (1-\kappa)\dot{\boldsymbol{z}}_{\boldsymbol{\lambda}}^{-}|_{ref} + \kappa\dot{\boldsymbol{z}}_{\boldsymbol{\lambda}}^{+}|_{ref} \tag{28}$$

where $\tilde{\boldsymbol{F}}_{\boldsymbol{AE}}|_B$ and $\tilde{\boldsymbol{M}}_{\boldsymbol{AE}}|_B$ are linear approximations from $\boldsymbol{F_{AE}}|_B$ and $\boldsymbol{M_{AE}}|_B$, respectively. The variables $\boldsymbol{z_\eta}|_{ref}$ and $\boldsymbol{z_\lambda}|_{ref}$ represent aeroelastic deformation and aerodynamic lag reduced–order states, respectively, expressed in the reference basis; the superscript (-) and (+) indicates the ROM whose speed is immediately lower and higher to the current, respectively; $\boldsymbol{\kappa}$ is responsible for weighing the contribution of each nearest ROM.

For ease of understanding consider that the aircraft flies at 14.2 m/s at a given time instant. In that time instant, $\dot{\boldsymbol{z}}^-$ will be calculated by using the ROM generated at 14 m/s and $\dot{\boldsymbol{z}}^+$ will be calculated by considering the ROM generated at 15 m/s. In that time instant, $\kappa = 14.2 - 14 = 0.2$, consequently the contribution of $\dot{\boldsymbol{z}}^-$ will be multiplied by a factor 0.8 while the contribution of $\dot{\boldsymbol{z}}^+$ will be multiplied by a factor 0.2.

It is important to notice that $\dot{\boldsymbol{z}}^-$ and $\dot{\boldsymbol{z}}^+$ must be expressed in the same basis of eigenvectors in order to perform arithmetic operation with both. Because of that, a reference basis must be elected arbitrarily (in the present work, we have chosen the ROM that describes the aeroelastic behavior around 15 m/s).

Consequently, in the beginning of every time step during simulation, a transformation of coordinates from the reference ROM basis to both nearest ROM basis must be performed by using the relation:

$$\boldsymbol{z'}^{\pm} = \bar{\boldsymbol{\Psi}}_{\pm}^{\boldsymbol{T}}\boldsymbol{\Phi}_{\boldsymbol{ref}}\boldsymbol{z} + \bar{\boldsymbol{\Psi}}_{\pm}^{\boldsymbol{T}}\bar{\boldsymbol{\Phi}}_{\boldsymbol{ref}}\bar{\boldsymbol{z}} \tag{29}$$

Then, the immediately higher and lower ROMs must be evaluated in their respective basis in order to obtain their first derivative vectors:

$$\dot{\boldsymbol{z}}_{\boldsymbol{\eta}}^{\boldsymbol{\prime}\pm} = \boldsymbol{\Lambda_\eta}\boldsymbol{z'_\eta} + \bar{\boldsymbol{\Psi}}_{\pm}^{\boldsymbol{T}}\boldsymbol{B}_{\boldsymbol{\eta}}^{\boldsymbol{RB}}\boldsymbol{u}_{\boldsymbol{\eta}}^{\boldsymbol{RB}} + \bar{\boldsymbol{\Psi}}_{\pm}^{\boldsymbol{T}}\boldsymbol{B}_{\eta}^{\lambda}\boldsymbol{u}_{\boldsymbol{\eta}}^{\boldsymbol{\lambda}} \tag{30}$$

$$\dot{\boldsymbol{z}}_{\boldsymbol{\lambda}}^{\boldsymbol{\prime}\pm} = \boldsymbol{\Lambda_\lambda}\boldsymbol{z'_\lambda} + \bar{\boldsymbol{\Psi}}_{\pm}^{\boldsymbol{T}}\boldsymbol{B}_{\boldsymbol{\lambda}}^{\boldsymbol{RB}}\boldsymbol{u}_{\boldsymbol{\lambda}}^{\boldsymbol{RB}} + \bar{\boldsymbol{\Psi}}_{\pm}^{\boldsymbol{T}}\boldsymbol{B}_{\lambda}^{\eta}\boldsymbol{u}_{\boldsymbol{\lambda}}^{\boldsymbol{\eta}} \tag{31}$$

After that, the ROM first derivative vectors must be transformed back to the reference basis:

$$\dot{\boldsymbol{z}}^{\pm}|_{ref} = \bar{\boldsymbol{\Psi}}^{\boldsymbol{T}}_{\boldsymbol{ref}} \boldsymbol{\Phi}_{\pm} \dot{\boldsymbol{z}}'^{\pm} + \bar{\boldsymbol{\Psi}}^{\boldsymbol{T}}_{\boldsymbol{ref}} \bar{\boldsymbol{\Phi}}_{\pm} \dot{\bar{\boldsymbol{z}}}'^{\pm} \tag{32}$$

Finally, Eq. (27) and Eq. (28) can be evaluated. Note that, for simplicity, the subscripts η and λ are omitted in Eq. (29) and in Eq. (32), however these equations are valid for both aeroelastic and aerodynamic lag ROMs.

6. RESULTS

In this section, two test cases are presented in order to compare FOM and ROM time responses. All the simulations were performed by using 4th–order Runge-Kutta method in a computer Intel Core I7-7700 3.6 GHz, 16 GB of RAM, Windows 10 and MATLAB 2018b. Table 1 shows a comparison between FOM and ROM simulation times for a 40s duration flight and indicates a significant simulation time reduction.

Table 1. Comparison between simulation time for a 40s duration flight.

Model	Order	Simulation Time (s)
FOM	269	454.8
ROM	57	23.1

The first test case shows a typical longitudinal maneuver and its objective is to compare longitudinal responses of FOM and ROM as well as verify that interpolated ROM can provide a good approximation when velocity changes significantly during flight.

The input controls are commanded in order to increase aircraft velocity from $15m/s$ to $19m/s$ (Fig. 3). A comparison between FOM and ROM longitudinal time responses is presented in Fig. 4 and the wing tip displacement is showed in the Fig. 5. The left wing tip displacement can be compared with Fig. 2, leading to the conclusion that the interpolation, in fact, overcame that limitation.

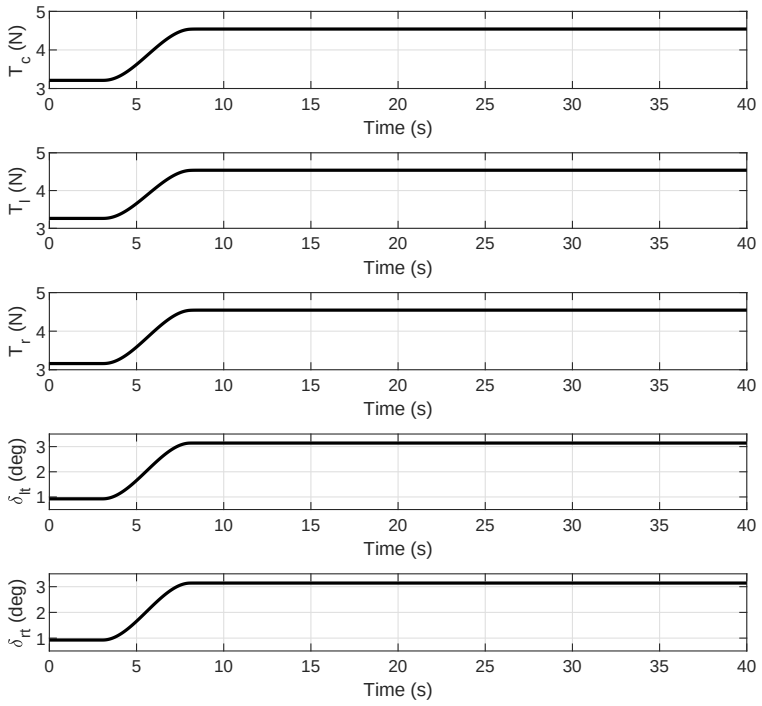

Figure 3. Longitudinal commands for a smooth change in velocity from 15 m/s to 19 m/s

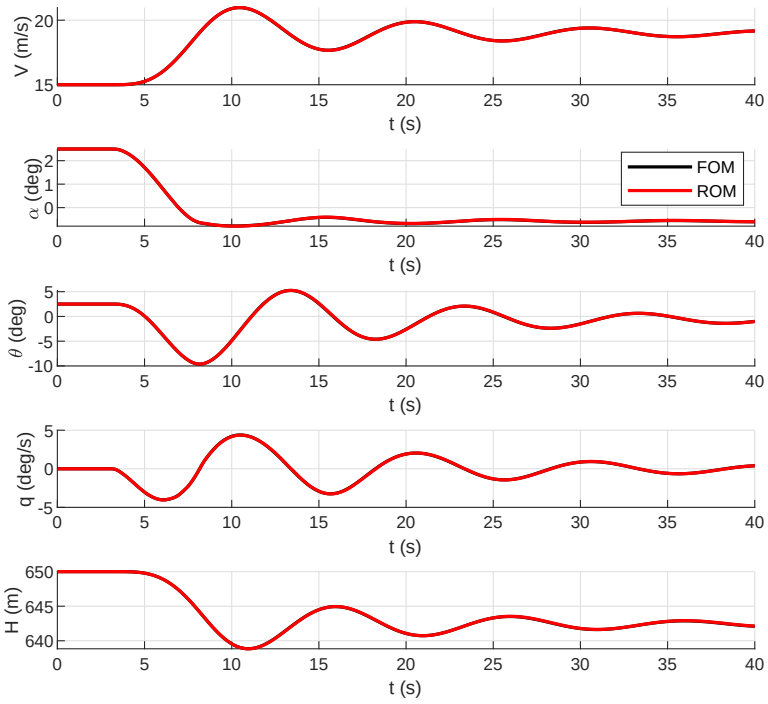

Figure 4. Longitudinal response for a smooth change in velocity from 15 m/s to 19 m/s

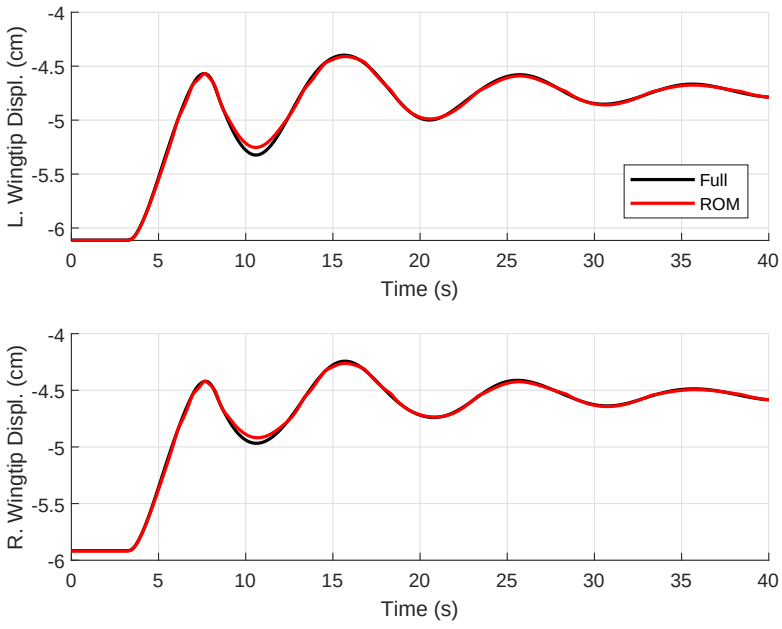

Figure 5. Wing tip displacement for a smooth change in velocity from 15 m/s to 19 m/s

In the second test case, the main objective is to compare lateral–directional responses between FOM and ROM. In order to do that, a rudder doublet was applied. Because X-HALE does not have any movable vertical lifting surface, the rudder effect is obtained by the application of differential thrusts in the external engines as showed in Fig. 6. The lateral–directional time response is presented in Fig. 7 and wing tip displacements are showed in Fig. 8. Again, the results show a good agreement between FOM and ROM.

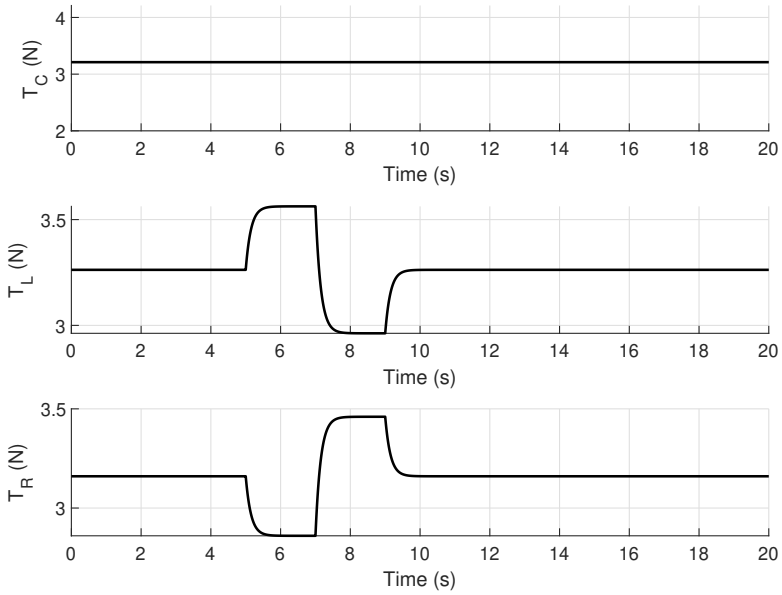

Figure 6. Rudder doublet excitation

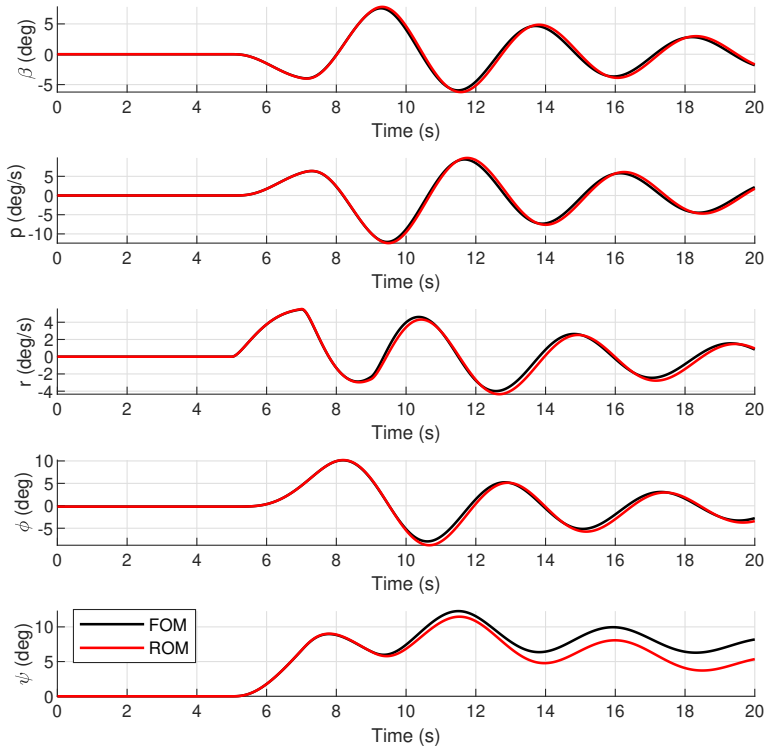

Figure 7. Rudder doublet lateral–directional response

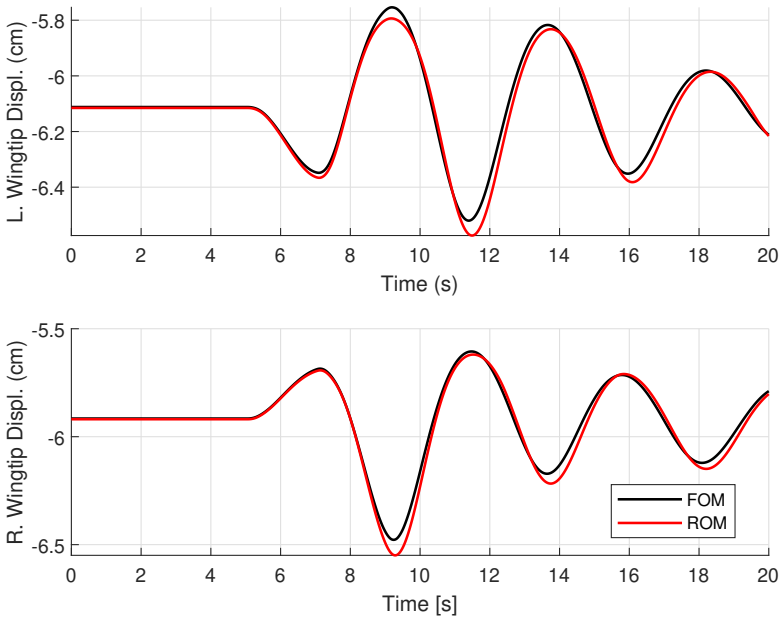

Figure 8. Rudder doublet wingtip displacement

7. CONCLUDING REMARKS

In this paper we presented an approach based on the interpolation of reduced–order models in order to reduce computational cost of flight simulation models of flexible aircraft, while keeping important aeroelastic features.

The method was applied to the X-HALE aircraft model, in the slightly flexible configuration (4m wingspan) and test cases were presented in order to compare FOM and ROM time responses for longitudinal and lateral–directional maneuvers.

The results show a good agreement between FOM and ROM, even when the latter is subjected to a significant variation of velocity, with expressive simulation time reduction.

8. ACKNOWLEDGEMENTS

This work has been funded by FINEP and EMBRAER under the research project Advanced Studies in Flight Physics, contract number 01.14.0185.00.

This study was financed in part by the Coordenação de Aperfeiçoamento de Pessoal de Nível Superior – Brasil (CAPES) - Finance Code 001.

9. REFERENCES

Cesnik, C.E.S., Senatore, P.J., Su, W. and Atkins, E.M., 2012. "X-hale: A very flexible unmanned aerial vehicle for nonlinear aeroelastic tests". *AIAA Journal*, Vol. 50, No. 12.

Da Ronch, A., Badcock, K., Wang, Y., Wynn, A. and Palacios, R., 2012. "Nonlinear model reduction for flexible aircraft control design". In *Proceedings of AIAA Atmospheric Flight Mechanincs Conference*.

Drela, M., 1989. "Xfoil: An analysis and design system for low reynolds number airfoils". *Lecture Notes in Engineering*, Vol. 54, pp. 1–12.

González, P., Boschetti, P., Cárdenas, E. and Amerio, A., 2010. "Evaluation of the flying qualities of a halfscale unmanned airplane via flight simulation". In *48th AIAA Aerospace Sciences Meeting Including the New Horizons Forum and Aerospace Exposition*. Florida, USA.

Guimarães Neto, A.B., Silva, R.G.A., Paglione, P. and Silvestre, F.J., 2016. "Formulation of the flight dynamics of flexible aircraft using general body axes". *AIAA Journal*, Vol. 54, No. 11.

Hedman, S.G., 1965. "Vortex lattice method for calculation of quasi steady state loadings on thin elastic wings". *Aeronautical Research Institute of Sweden, Report 105*.

Kaden, A., Boche, B. and Luckener, R., 2013. "Hardware-in-the-loop flight simulator - an essential part in the development process for the automatic flight control system of a utility aircraft." *Advances in Aerospace Guidance, Navigatin and Control*, pp. 585–601.

Kish, B.A., Leggett, D.B., Nguyem, B.T., Cord, T.J. and Slutz, G.J., 1996. "Concepts for detecting pilot–induced–oscillation using manned simulation". In *21st Atmospheric Flight Mechanics Conference, Guidance, Navigation, and Control and Co-located Conferences*. pp. 559–568.

Livne, E., 2003. "Future of airplane aeroelasticity". *Journal of Aircraft*, Vol. 40, No. 6, pp. 1066–1092.

Paulino, J.A., Da Ronch, A., Guimarães Neto, A.B., Silvestre, F.J. and Morales, M.A.V., 2018. "On real–time simulation of flexible aircraft with physics–derived models". In *Proceedings of 31st Congress of the International Council of the Aeronautical Sciences*. Belo Horizonte, Brazil.

Paulino, J.A., Silvestre, F.J., Guimarães Neto, A.B., Monteiro, T.P., Annes da Silva, R.G. and Da Ronch, A., 2017. "Application of nonlinear model order reduction technique to a flexible aircraft for real–time simulations". In *International Forum on Aeroelasticity and Structural Dynamics*. Como, Italy.

Shearer, C.M. and Cesnik, C.E.S., 2007. "Nonlinear flight dynamics of very flexible aircraft". *Journal of Aircraft*, Vol. 44, No. 5, p. 1528.

Silvestre, F.J., 2013. *Methodology for Modeling the Dynamics of Flexible, High-Aspect-Ratio Aircraft in the Time Domain for Aeroservoelastic Investigations*. Ph.D. thesis, TU Berlin, Berlin, Germany.

Silvestre, F.J. and Luckner, R., 2015. "Experimental validation of a flight simulation model for slightly flexible aircraft". *AIAA Journal*, Vol. 1, No. 1, pp. 1–17.

Wagner, H., 1925. "über die entstehung des dynamischen auftriebes von tragflügeln". *Zeitschrift für angewandte Mathematik und Mechanik*, Vol. 5.

Waszak, M.R. and Schmidt, D.K., 1988. "Flight dynamics of aeroelastic vehicles". *Journal of Aircraft*, Vol. 25, No. 6, pp. 563–71.

Waszniowski, L., Hanzalek, Z. and Doubrava, J., 2011. "Aircraft control system validation via hardware–in–the–loop simulation". *Journal of Aircraft*, Vol. 48, No. 4, pp. 1466–1468.

10. RESPONSIBILITY NOTICE

The authors are the only responsible for the printed material included in this paper.